Ultramicroscopy 196 (2019) 161–166

Contents lists available at ScienceDirect

Ultramicroscopy

journal homepage: www.elsevier.com/locate/ultramic

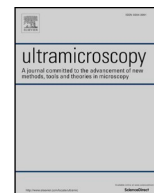

Charging of electron beam irradiated amorphous carbon thin films at liquid nitrogen temperature

Simon Hettler*[,a], Jo Onoda[b], Robert Wolkow[b], Jason Pitters[c], Marek Malac[b,c]

[a] Laboratory for Electron Microscopy, Karlsruhe Institute of Technology, Engesserstrasse 7, Karlsruhe 76131, Germany
[b] Department of Physics, University of Alberta, 11421 Drive, Edmonton, Saskatchewan T6G 2E1, Canada
[c] Nanotechnology Research Centre, National Research Council, 11421 Drive, Edmonton, Saskatchewan T6G 2M9, Canada

ARTICLE INFO

Keywords:
Electron-beam induced charging
Thin film
Phase plate
Radiation damage
Hole free phase plate
Volta phase plate
Transmission electron microscope

ABSTRACT

We studied the charging behavior of an amorphous carbon thin film kept at liquid-nitrogen temperature under focused electron-beam irradiation. Negative charging of the thin film is observed. The charging is attributed to a local change in the work function of the thin film induced by electron-stimulated desorption similar to the working principle of the hole free phase plate in its Volta potential implementation at elevated temperature. The negative bias of the irradiated film arises from the electron beam induced desorption of water molecules from the carbon film surface. The lack of positive charging, which is expected for non-conductive materials, is explained by a sufficient electrical conductivity of the carbon thin film even at liquid-nitrogen temperature as proven by multi-probe scanning tunneling microscopy and spectroscopy measurements.

1. Introduction

Amorphous carbon (aC) thin films are one of the most frequently used sample supports in transmission electron microscopy (TEM). aC exhibits many beneficial characteristics such as sufficient electrical conductivity, low electron scattering coefficients and mechanical stability. Furthermore, aC can be fabricated in a large number of different varieties. Due to these properties, aC is often used as supporting structure, e.g., in cryo-TEM [1] or for nanoparticle investigations. In addition, physical phase plates (PPs) for phase-contrast TEM typically consist of an aC film with a central hole [2]. If positioned accordingly, PPs induce a relative phase shift between the scattered and unscattered part of the electron wave and thus enhance the phase contrast. Despite its sufficient conductivity, PP experiments showed that aC is prone to a more subtle type of charging even at elevated temperatures [3]. This charging phenomenon can be explained by a change in the work function of the thin film induced by electron-stimulated desorption of adsorbed species [4] and is exploited by the concepts of the hole-free PP (HFPP) [5,6].

When the thin-film conductivity is sufficiently high and insulating layers are not present, the beam-induced charging can exhibit a negative polarity. The negative polarity is in contrast to the observed positive charging of non-conductive materials such as vitrified ice, silicon nitride or contamination on carbon films near room temperature caused by the emission of secondary electrons (SEs) [5,7,8]. Although charging of vitrified ice specimens in cryo-experiments is reduced in vicinity of the aC support film, it was also reported that the aC thin film itself is charging positively due to its poor conductivity at liquid-nitrogen temperature [9,10]. Since cryo-specimens consist of an aC thin film encapsulated in a substantial amount of vitrified ice, it is not clear whether the aC thin film itself or the insulating ice is causing the positive charge.

Here, we analyze the charging of an as-prepared aC thin film at liquid nitrogen (LN_2) temperature under intense electron-beam irradiation to assess the inherent properties of aC without the effect of embedding in vitrified ice. We observed negative charging of the aC thin film which can be explained by the same model which is responsible for the functionality of HFPPs at elevated temperature [4]. As this model requires an aC thin film with sufficient electrical conductivity, we performed conductivity measurements of aC thin films at LN_2 temperature using multi-probe scanning tunneling microscopy (STM). The experimental results indicate that the conductivity of aC is strongly increased when irradiated with electrons. Using a HFPP at LN_2 temperature could be important for cryo-TEM applications as it eliminates the need to have a heated PP in the vicinity of a cryo sample.

2. Materials and methods

The TEM investigations and related analysis procedures were conducted as described previously [4,11,12]. We performed the

* Corresponding author.
E-mail address: simon.hettler@kit.edu (S. Hettler).

https://doi.org/10.1016/j.ultramic.2018.10.010
Received 15 August 2018; Accepted 25 October 2018
Available online 29 October 2018
0304-3991/ © 2018 Published by Elsevier B.V.

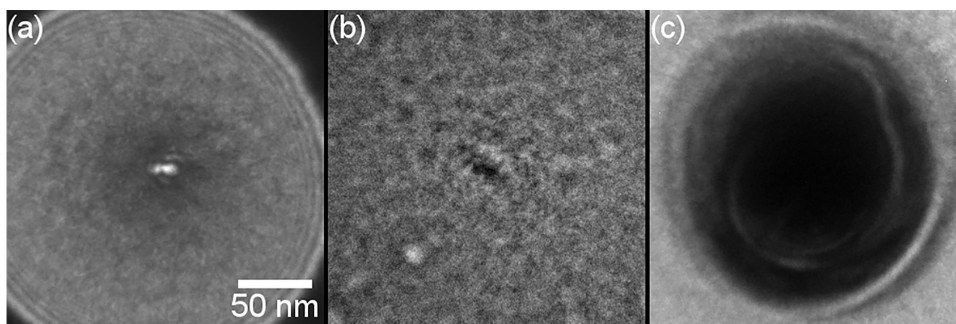

Fig. 1. TEM images of the aC thin film acquired under strong overfocus conditions after focused electron-beam irradiation (a) shortly after insertion in the microscope, (b) at LN_2 temperature and (c) after warming up to room temperature. (a) Contamination is visible as a bright spot on the thin film. (b) A dark spot stemming from both negative charging and the removal of material is observed at LN_2 temperature. (c) A huge amount of contamination is deposited on the thin film after returning to room temperature.

measurements using a Hitachi HF−3300 (Hitachi High Technologies, Naka, Japan) equipped with a cold field emission gun operated at 300 keV. The instrument is fully dry pumped with a pressure of about $3{\cdot}10^{-8}$ Torr near the sample. The column is baked at least 60 h per week and a UV cleaner [13] is utilized to remove residual contamination inside the microscope vacuum. An additional test specimen was implemented in the condenser lens system above the standard sample plane. Electron optics was adjusted in a way, that the back focal plane of the test specimen coincides with the standard sample plane. In this setup, the aC thin film, which is positioned in the sample plane using a cryo-specimen holder (Gatan Inc, Pleasanton, CA, USA) to study charging effects at LN_2 temperature, is irradiated with a focused and intense electron beam. Two alternative setups of the imaging lens system allow the acquisition of series of electron energy loss (EEL) spectra or HFPP images of the test specimen with the aC thin film working as PP. The experimental data is analyzed to extract information on changes in the relative thickness of the aC thin film and on the polarity and amount of charge built up on the aC thin film. We refer to our previous publications for further details on the setup and on the data analysis [4,11,14].

The aC thin film was fabricated by electron-beam evaporation of C onto a freshly cleaved mica substrate using a custom built, cryo pumped vacuum evaporator. The thin film is transferred onto Cu grids (Ted Pella, Reading, CA, USA) by floating on water and was not treated to inhibit contamination. HFPP images and EEL spectra were recorded under three different experimental conditions: The first set of series was acquired at room temperature (RT) shortly after insertion of the aC thin film in the microscope. In the following experiment, the aC thin film was cooled to LN_2 temperature and the second set of series was recorded after the sample holder temperature and mechanical drift settled. The effect of a beam shower was studied by irradiation of a large area of the film around the region of interest with a 300 keV beam with total areal doses below 0.15 $C{\cdot}cm^{-2}$. Finally, the last series was acquired at RT shortly after warming up from LN_2 temperature. aC thin films prepared in the same batch were also studied using multi-probe STM. Two probe electrical measurements were performed with an Omicron Nanoprobe (Scienta Omicron Inc), operated at 77 K. The background pressure of the system was $3{\cdot}10^{-11}$ Torr. The sample was mechanically mounted on an STM sample plate using mechanical clips. No degassing of the sample was performed prior to study in the nanoprobe instrument. The STM probes were brought into tunneling contact by regulating the tip height using the tunnel current as feedback. Stable tunneling current was routinely achieved with stationary tips, however, STM imaging of the sample was not possible because of unstable tunnel current that resulted during the XY scanning of the tip. This is attributed to the flexible nature of the aC films.

In order to contact the sample for electrical measurement, the probes were overdriven into the sample by 5 nm. This assured repeatable, light contact with the aC thin film during measurements of the freestanding sample. In order to measure probe to probe current, the sample was electrically removed from the circuit. Probe to probe measurements were performed with one grounded probe and one probe with an applied bias. Current was measured at both probes and correlated well between the probes. The probes were spaced $\approx 30\ \mu m$ apart.

Electron exposure of the sample was performed using a scanning electron microscope. The exposure region included the probes and was $110 \times 59\ \mu m^2$. The probe position was not changed between exposures, ensuring consistent contact to the sample. Thermal drift was minimal and did not affect the measurements. The exposure current of 2 nA at 10 kV was calibrated using a Faraday cup and an exposure irradiation dose was determined from the exposed area, time and known current.

3. Experimental results

3.1. TEM investigations

The experimental results obtained from the TEM investigations are shown in Figs. 1 and 2. Fig. 1 depicts three TEM images of the aC thin film after acquisition of a series of EEL spectra under the three different experimental conditions. The results from the data analysis are displayed in Fig. 2. Contamination builds up on the thin film if irradiated shortly after insertion in the microscope which can be recognized by the bright spot in Fig. 1a and the increasing relative thickness (blue line in Fig. 2a). The acquisition of a HFPP image series shows that the buildup of contamination induces a positive phase shift (not shown) arising from the increasing thickness of the thin film [11].

Rather than an increase of the aC thickness, a slight decrease is observed if the aC thin film is irradiated while at LN_2 temperature (red line in Fig. 2a). The decrease in thickness is better visualized by a comparison between the initial and the final EEL spectrum of the series (Fig. 2b), where the final EEL spectrum exhibits a lower intensity in the low-loss region. Fitting the aC plasmon peak after zero-loss subtraction [15] yields a plasmon energy $E_P = 26 \pm 1$ eV independent of the areal dose which indicates that a structural change of the aC thin film does not occur. The experimental results obtained from the determination of the induced phase shift are depicted in Fig. 2c. A negative phase shift, corresponding to a negative charge/potential on the aC film, is observed when the aC thin film kept at LN_2 temperature is irradiated (blue line in Fig. 2c). The magnitude of phase shift increases rapidly up to an areal dose of $\approx 50\ C{\cdot}cm^{-2}$ before the rate starts to level off. However, the magnitude of phase shift does not reach a plateau within our measurement range of up to 300 $C{\cdot}cm^{-2}$ but continues to increase until the end of the series up to a value of $-0.6\ \pi$.

The magnitude of the induced phase shift is influenced by applying a beam shower immediately before the acquisition of a series. The measured phase shift after focused irradiation with a dose of 300 $C{\cdot}cm^{-2}$ decreases from $-0.6\ \pi$ (no beam shower) to $-0.5\ \pi$ and $-0.4\ \pi$ for beam shower times of 30 and 60 s, respectively. To obtain further information on the phase shift evolution, it can be fitted by a double asymptotic function ϕ in dependence of the areal dose q [6]:

$$\phi(q) = \phi_1{\cdot}\left(1 - e^{-q/q_1}\right) + \phi_2{\cdot}\left(1 - e^{-q/q_2}\right) \tag{1}$$

$\phi_{1,2}$ are the saturation phase shifts and $q_{1,2}$ are the characteristic doses. The fit to the evolution without beam shower is plotted as a

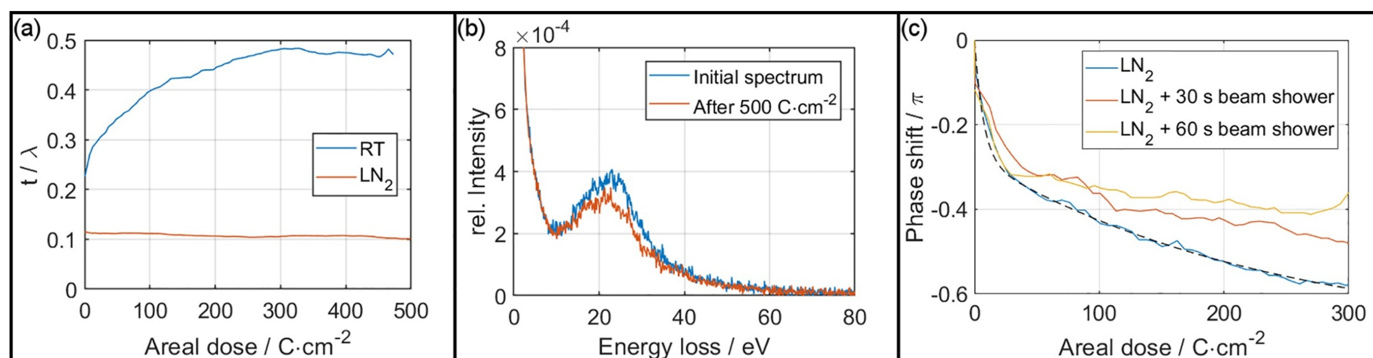

Fig. 2. Experimental results obtained from series of EEL spectra and HFPP image series. (a) The relative thickness of the investigated aC thin film increases strongly with the areal dose when irradiated at RT due to the buildup of contamination (blue line). A minor decrease in thickness is observed at LN_2 temperature which can be attributed to a removal of an adsorbed ice layer (red line). (b) EEL spectra from the beginning (blue) and the end (red) of a series show that material is indeed removed from the thin film. (c) A negative phase shift of up to -0.6 π is measured if the aC thin film is irradiated at LN_2 temperature (blue line). The amount decreases, if a large area of the thin film is irradiated with a beam shower just before the acquisition of the series. A double asymptotic function can be fitted to the evolution which is displayed for the case without beam shower (dashed black line). (For interpretation of the references to colour in this figure legend, the reader is referred to the web version of this article.)

dashed line in Fig. 2c. Due to the very fast rise of the phase shift and the noise in the phase shift determination, the error on the fit parameters is high. Nevertheless, the fit gives an estimation of the characteristic doses, which are $q_1 < 10\ \mathrm{C\cdot cm^{-2}}$ and $q_2 \approx 200\ \mathrm{C\cdot cm^{-2}}$. The sum of the saturation phase shifts $\phi_1 + \phi_2$ decreases with increasing beam shower time.

The TEM image of the thin film after acquisition of the series at LN_2 temperature shows a dark spot which is in contrast to the bright spot observed for a contaminating thin film (Fig. 1). After warming up to RT, contamination recurs much faster than on a pristine film and the collection of the EEL spectra and HFPP image series was impossible due to almost complete obstruction of the electrons by the deposited contamination almost immediately after the beam is unblanked. Although the beam diameter and current density on the aC thin film is identical to the previous measurements, the contamination spot is much larger (Fig. 1c) than for either experiments without LN_2 cooling analyzed soon after insertion in the microscope vacuum [11].

3.2. Conductivity measurements

Fig. 3 shows the results obtained by STM measurements. The I/V spectroscopy data collected between the two probes is plotted in Fig. 3b for different electron irradiation doses. After the initial contact with the probes at time zero, the I/V data shows little current. After 5 min of waiting for drift to settle, a repeated I/V curve shows virtually no change in the characteristics of the film, indicating that drift or changes in the contact were not a concern. The focused electron beam was then exposed to the aC thin film. A 10 kV and 2 nA probe was scanned over a region of $\approx 6500\ \mu\mathrm{m}^2$, which included the I-V probes. Spectroscopy data was acquired at 3.5, 7, 9, 20, 40 and 60 min and the corresponding electron exposure doses were calculated to be 0.0065, 0.013, 0.017, 0.037, 0.074 and 0.111 $\mathrm{C\cdot cm^{-2}}$. It is clear from the spectroscopy data that the electrical properties of the film have been altered by the electron exposure. Some noise and variability is visible in the spectra and may be related to the film flexibility or contacts at the probes, but a general trend of film conductivity increase with electron exposure is evident.

4. Discussion

The experimental results give an insight in the properties of LN_2-cooled aC films under electron-beam irradiation and provide information on the relative strength of the processes responsible for the film charging and contamination. Contamination describes material transport and buildup due to cross linking of adsorbed molecules supplied by surface diffusion along the thin-film surface [11,16]. We observed contamination shortly after insertion of the thin film but not after cooling the thin film to LN_2 temperature (Fig. 1a and b). The reason is that the surface diffusion and thus the buildup of contamination is inhibited at a low temperature, although the number of adsorbed molecules on the thin film increases by absorption from residual gases in the microscope vacuum on the cooled thin-film surface. A large amount of the adsorbed molecules remains on the thin film, even after warming up to RT. This is witnessed by the drastic increase in contamination rate and thickness in experiments performed after warming up to RT, which blocks the electron beam almost completely after a rather small irradiation dose (Fig. 1c).

A second process is material removal by electron-stimulated desorption [4,17–19] as well as knock-on electron beam induced sputtering [7]. When the aC thin film is irradiated at LN_2 temperature, adsorbed molecules are locally desorbed leading to a reduced number of inelastically scattered electrons (Fig. 2b). Assuming that the desorbed species are water molecules, as expected for a vacuum system that is pumped by a turbo molecular pump (supplementary material of [4]), the thickness of the removed layer can be estimated to be about 1 nm. This thickness decrease is not sufficient to explain the observed negative phase shift from the thickness decrease alone (Fig. 2c) indicating that an additional effect is present. The origin of the negative phase shift is attributed to the change in work function of the aC thin film due to the electron-stimulated desorption of adsorbed molecules as described in [4].

Adsorbed (water) molecules decrease the work function of the aC thin film [20]. If the molecules are desorbed by the intense electron beam, the work function is restored to the original value of aC which is equal to assuming a negative potential δV in the irradiated area. According to the established model in [4], the induced phase shift is given by

$$\phi = C_E \cdot \delta V \cdot R \qquad (2)$$

with R being the radius of the irradiated patch, $\delta V < 0$ the negative potential and C_E the interaction constant. Fig. 4 shows a schematic review of the model. Initially, the aC thin film is covered by a thin layer of adsorbed water molecules (Fig. 4a). The thickness can be estimated to be around 1–2 monolayers on both sides, as the material removed by the electron beam is calculated to be approximately 1 nm of water (c.f. Fig. 2b). If the thin film is now irradiated with the electron beam, the water layer in the area of the intense zero-order beam is removed by electron-stimulated desorption and the central patch exhibits a negative potential. This requires only a small dose which corresponds to the first characteristic dose q_1 of the fit function to the phase shift (Eq. (1) and

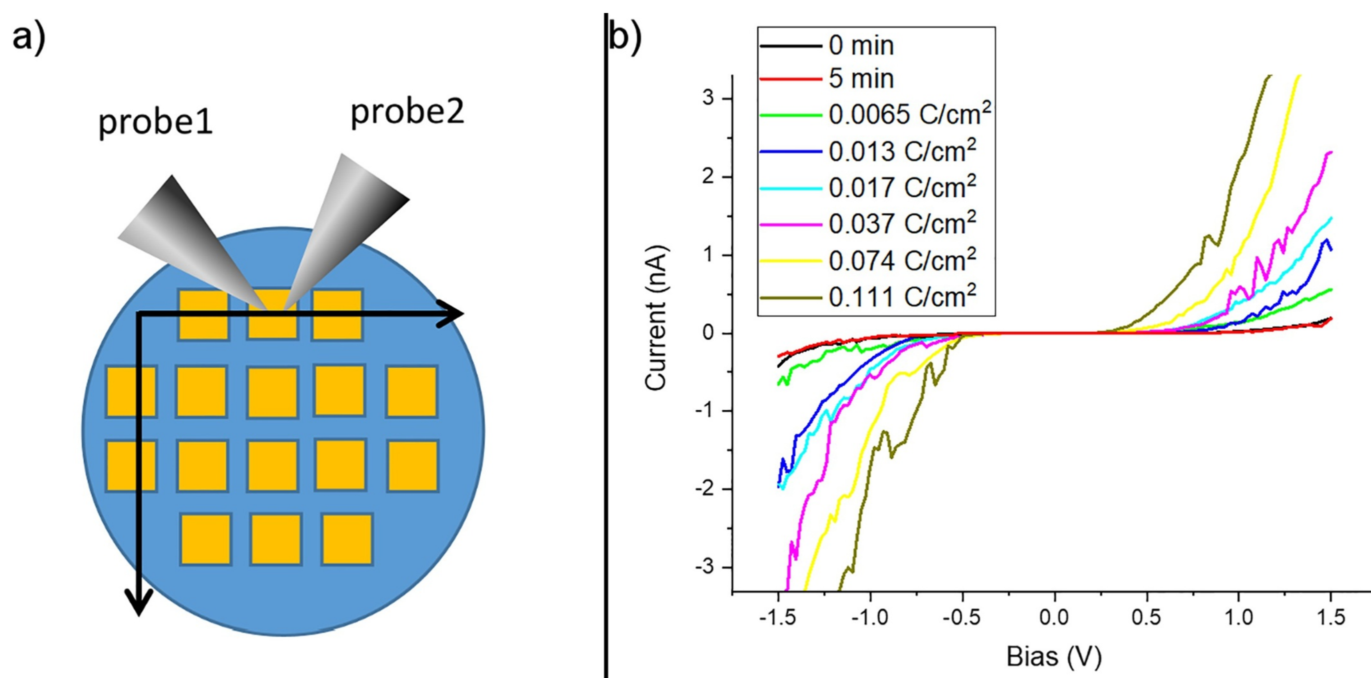

Fig. 3. (a) Schematic of the two probe experiment conducted by STM. The two probes were placed $\approx 30\ \mu$m apart on the aC thin film (orange) freestanding between the Cu grid bars (blue). b) Probe to probe I/V spectroscopy data collected for different electron exposure doses. The increasing conductivity with increasing electron dose is evident. (For interpretation of the references to colour in this figure legend, the reader is referred to the web version of this article.)

Fig. 2c).

The further increase of the negative phase shift can be attributed to an increasing radius R of the patch. This increase is induced by primary electrons scattered in the sample which can generate SEs also outside the zero-order beam and by SEs generated in the area of the zero-order beam which propagate to surrounding areas [21]. These SEs cause desorption of molecules in an area around the patch - however with a much lower rate. This leads to a slow increase in the diameter of the patch and can be linked to the second characteristic dose q_2 of the asymptotic function (Eq. (1)).

The application of a beam shower prior to the acquisition of a series decreases the amount of measurable phase shift (Fig. 2c). During a beam shower, a large area of the thin film is irradiated with 300 keV electrons, which can cause electron-stimulated desorption of whatever species are present on the surface of the film. The beam shower thus effectively increases the work function of the aC thin film in a large area, albeit not to the clean aC surface value at the low doses implemented here. If the aC thin film is then further irradiated with a focused electron beam, the difference between the work function in the irradiated patch and the surrounding thin film is reduced compared to the situation without beam shower. This leads to a reduction of the attainable δV and the observed amount of relative phase shift between the scattered and unscattered part of the electron wave is reduced (Fig. 2c).

The model based on the change in work function due to water removal by electron-stimulated desorption requires an underlying thin film with adequate electrical conductivity. Therefore we assume, that an aC thin film exhibits a sufficient conductivity to compensate for any SE that left the thin film. Indeed, the multi-probe STM measurements show that the conductivity of aC at LN_2 temperature increases after irradiation with electrons. At this point we can only speculate about the physical reason for the conductivity enhancement. A possible explanation could be that SEs generated by the primary electron beam in the aC thin film cause desorption and diffusion from H_2. H_2 has an important influence on ultra nanocrystalline diamond [22] and could passivate conduction paths in the thin film, which are restored during electron irradiation. Independent of the correct physical explanation, which is not the aim of this paper, the multi-probe STM results prove that the aC thin film provides the necessary conductivity.

The energy of the irradiating electrons is only 10 keV in the multi-probe STM experiment compared to 300 keV in TEM. The SE yield decreases with primary electron energy E with $E^{-0.8}$ [23], which leads to a dose necessary to generate the same amount of SE which is a factor of 15 higher in TEM. The necessary dose at 300 keV can be estimated to be below 1 $C \cdot cm^{-2}$ which is reached already before the first data point in the phase shift measurements (c.f. Fig. 2c).

The results show that aC is not charging positively at LN_2 temperature. If only a thin layer of molecules (1 nm), which are assumed to

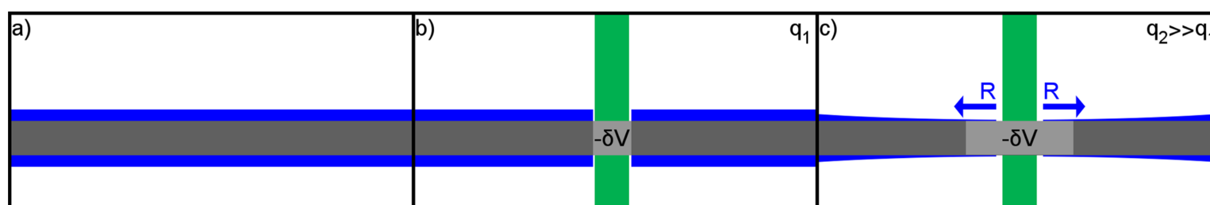

Fig. 4. Schematic description of the buildup of a negative phase shift. (a) Initially, the aC thin film is covered with a thin adsorbed water layer of homogeneous thickness. (b) The area irradiated with the intense zero-order beam is dried almost instantaneously by desorption of the water leading to a negative potential δV. This process requires only little areal dose q_1. (c) The water is desorbed around the central patch by SEs generated by primary electrons scattered in the sample. The necessary dose q_2 to reach an equilibrium state is sufficiently higher.

be mainly water molecules due to the typical composition of the residual gas atmosphere in the microscope [4], is adsorbed on the thin film, the observed phase shift under irradiation with a focused electron beam is negative. For real cryo-TEM samples, the thickness of the vitrified ice layer is much higher than a few monolayers discussed here. Although vitrified ice is thinned under electron irradiation [24], the ice layer itself can charge positively until it is completely removed by electron-stimulated desorption which is probable for the low electron doses in cryo-TEM [10]. Additionally, the low doses (typically $\leq 0.2\ \mathrm{C \cdot cm^{-2}}$) might not be sufficient to induce a conductivity increase that is high enough to prevent positive charging of the aC thin film itself.

When comparing the current results at LN_2 temperature to recent work published on HFPPs and Volta PPs, the observed phase shift evolution agrees well with the results from Danev and Marko obtained at about 200 °C [6,25]. The strong difference in necessary temperature to reach the same phase shift can be explained by two aspects, namely the different pressures in the microscopes and the diameter of the irradiating electron beam. While the Hitachi HF−3300 provides pressures of $3 \cdot 10^{-8}$ Torr due to regular column baking, typical pressures in cryo microscopes are at least one magnitude higher and may still contain significant amount of water vapour. The low pressure is also likely the reason, why we only observed a very low phase shift at elevated temperatures in our previously published results [4]. A second strong impact on the amount of observed negative phase shift is the diameter of the irradiating electron beam [4]. As we used the condenser lens system to create the irradiating beam, the diameter was 20 nm while it can easily be in the range of a few hundreds of nm in the back focal plane when using conventional TEM imaging [5].

5. Summary

We studied the charging behavior of an amorphous carbon (aC) thin film at liquid nitrogen (LN_2) temperature. The experimental results are summarized in the following:

- A negative phase shift is measured when the aC thin film cooled down to liquid nitrogen temperature is irradiated with a focused electron beam. The origin of the phase shift is a change in work function of the aC thin film due to removal of a thin layer of adsorbed molecules by electron-stimulated desorption [4]. Applying a beam shower prior to the measurement reduces the observed negative phase shift.
- The model describing the observed negative phase shift requires an underlying thin film with sufficiently high electrical conductivity. Multi-probe scanning tunneling microscopy measurements show that aC fulfills this condition if it is irradiated by electrons.
- Contamination is efficiently inhibited by sample cooling which however comes at the expense of the adsorption of a large number of molecules on the thin film. Contamination is therefore drastically increased once the thin film is warmed up again.
- The charging behavior of pure aC thin films differs largely from cryo specimens, i.e. an aC thin film encapsulated by vitrified ice, which may charge positively.

Our results allow conclusions on the operation of hole-free phase plates (HFPPs). Contamination has to be inhibited to obtain the negative potential which can be done, e.g., by heating or by cooling down to liquid nitrogen temperature or by using a zero-order beam with a large diameter [26]. The phase shift magnitude and evolution will depend on numerous conditions such as thin-film temperature and roughness, microscope pressure and residual gas composition, current and diameter of the focused electron beam as well as on the scattering properties of the sample. Due to these dependencies, the operation mode of a HFPP is expected to be different for different microscopes and should be calibrated in detail for each application to get optimum phase contrast of the sample. The possibility to use a thin film held at LN_2 temperature as HFPP may benefit phase plate cryo electron microscopy by eliminating a heated phase plate hardware in close proximity of a cryo sample.

Acknowledgments

S. Hettler acknowledges funding from the Carl-Zeiss-Stiftung and thanks Prof. D. Gerthsen for her ongoing support. The work at NRC-NANO was supported by the National Research Council of Canada. The ongoing support of Hitachi High Technologies (Naka, Japan) especially Dr. Y. Taniguchi and Hitachi High Technologies Canada (D. Hoyle and C. Soong) was crucial in developing a custom experimental setup of the Hitachi HF−3300. Collaboration with JEOL Ltd. and JEOL USA Inc. allowed us to pursue phase-plate development at NRC-NANO. In particular the help of Dr. M. Kawasaki (JEOL USA Inc.) and Dr. Y. Okura, Dr. S. Motoki, Dr. I. Ishikawa and Dr. Y. Konyuba (JEOL Ltd.) has been crucial in developing the phase plate expertize at NRC-NANO. Discussions with Prof. Ray Egerton and Prof. Marco Beleggia were critical in understanding charging of thin films.

References

[1] C.J. Russo, L.A. Passmore, Progress towards an optimal specimen support for electron cryomicroscopy, Curr. Opin. Struc. Biol. 37 (2016) 81–89, https://doi.org/10.1016/j.sbi.2015.12.007.
[2] R. Danev, K. Nagayama, Transmission electron microscopy with zernike phase plate, Ultramicroscopy 88 (4) (2001) 243–252, https://doi.org/10.1016/S0304-3991(01)00088-2.
[3] R. Danev, R.M. Glaeser, K. Nagayama, Practical factors affecting the performance of a thin-film phase plate for transmission electron microscopy, Ultramicroscopy 109 (4) (2009) 312–325, https://doi.org/10.1016/j.ultramic.2008.12.006.
[4] S. Hettler, E. Kano, M. Dries, D. Gerthsen, L. Pfaffmann, M. Bruns, M. Beleggia, M. Malac, Charging of carbon thin films in scanning and phase-plate transmission electron microscopy, Ultramicroscopy 184 (Pt A) (2018) 252–266, https://doi.org/10.1016/j.ultramic.2017.09.009.
[5] M. Malac, M. Beleggia, M. Kawasaki, P. Li, RayF. Egerton, Convenient contrast enhancement by a hole-free phase plate, Ultramicroscopy 118 (03043991) (2012) 77–89, https://doi.org/10.1016/j.ultramic.2012.02.004.
[6] R. Danev, B. Buijsse, M. Khoshouei, J.M. Plitzko, W. Baumeister, Volta potential phase plate for in-focus phase contrast transmission electron microscopy, PNAS 111 (44) (2014) 15635–15640, https://doi.org/10.1073/pnas.1418377111.
[7] R.F. Egerton, P. Li, M. Malac, Radiation damage in the TEM and SEM, Micron 35 (6) (2004) 399–409, https://doi.org/10.1016/j.micron.2004.02.003.
[8] J. Cazaux, From the physics of secondary electron emission to image contrasts in scanning electron microscopy, J. Electron. Microsc. 61 (5) (2012) 261–284, https://doi.org/10.1093/jmicro/dfs048.
[9] J. Brink, M.B. Sherman, J. Berriman, W. Chiu, Evaluation of charging on macromolecules in electron cryomicroscopy, Ultramicroscopy 72 (1998) 41–52, https://doi.org/10.1016/S0304-3991(97)00126-5.
[10] C.J. Russo, R. Henderson, Charge accumulation in electron cryomicroscopy, Ultramicroscopy 187 (2018) 43–49, https://doi.org/10.1016/j.ultramic.2018.01.009.
[11] S. Hettler, M. Dries, P. Hermann, M. Obermair, D. Gerthsen, M. Malac, Carbon contamination in scanning transmission electron microscopy and its impact on phase-plate applications, Micron 96 (2017) 38–47, https://doi.org/10.1016/j.micron.2017.02.002.
[12] M. Malac, R.A. McLeod, P. Li, W.C. Bigelow, J.Y. Howe, L.F. Allard, Y. Taniguchi, M.S. Moreno, Fast mechanical shutter in hitachi HF 3300, a 60 kv to 300 kv TEM, Microsc Microanal 16 (S2) (2010) 338–339, https://doi.org/10.1017/S1431927610055777.
[13] C. Soong, P. Woo, D. Hoyle, Contamination cleaning of TEM/SEM samples with the ZONE cleaner, Micros. Today 20 (06) (2012) 44–48, https://doi.org/10.1017/S1551929512000752.
[14] M. Malac, S. Hettler, M. Hayashida, M. Kawasaki, Y.O. Konyuba, Y. Okura, H. Iijima, I. Ishikawa, M. Beleggia, Computer simulations analysis for determining the polarity of charge generated by high energy electron irradiation of a thin film, Micron 100 (2017) 10–22, https://doi.org/10.1016/j.micron.2017.03.015.
[15] R.F. Egerton, Electron energy-loss spectroscopy in the electron microscope, 3rd ed., The language of science, Springer, New York, 2011.
[16] J.J. Hren, Specimen contamination in analytical electron microscopy: sources and solutions, Ultramicroscopy 3 (1979) 375–380, https://doi.org/10.1016/S0304-3991(78)80057-6.
[17] E.M. Williams, J.L. de Segovia, Electron stimulated desorption of ions from surfaces: techniques, methodology and some recent findings with water at metals and semiconductors, Vacuum 39 (7/8) (1989) 633–642, https://doi.org/10.1016/0042-207X(89)90006-7.
[18] R.D. Ramsier, J.T. Yates, Electron-stimulated desorption: principles and applications, Surf. Sci. Rep. 12 (1991) 243–378, https://doi.org/10.1016/0167-5729(91)

90013-N.
[19] W.F. van Dorp, T.W. Hansen, J.B. Wagner, J.T.M. De Hosson, The role of electron-stimulated desorption in focused electron beam induced deposition, Beilstein. J. Nanotechnol. 4 (2013) 474–480, https://doi.org/10.3762/bjnano.4.56.
[20] M.A. Henderson, The interaction of water with solid surfaces: fundamental aspects revisited, Surf. Sci. Rep. 46 (2002) 1–308, https://doi.org/10.1016/S0167-5729(01)00020-6.
[21] R.F. Egerton, M. Malac, The lateral range and energy deposition of fast secondary electrons, Microsc. Microanal. 10 (S02) (2004) 1382–1383, https://doi.org/10.1017/S1431927604880541.
[22] X.J. Hu, X.H. Chen, J.S. Ye, The roles of hydrogen in the diamond/amorphous carbon phase transitions of oxygen ion implanted ultrananocrystalline diamond films at different annealing temperatures, AIP Adv. 2 (4) (2012) 042109, https://doi.org/10.1063/1.4759087.
[23] L. Reimer, Scanning Electron Microscopy: Physics of Image Formation and Microanalysis, Volume 45 of Springer Series in Optical Sciences, 2nd ed., Springer, Heidelberg, 2010.
[24] J. Berriman, K.R. Leonard, Methods for specimen thickness determination in electron microscopy, Ultramicroscopy 19 (4) (1986) 349–366, https://doi.org/10.1016/0304-3991(86)90095-1.
[25] M. Marko, C. Hsieh, E. Leith, D. Mastronarde, S. Motoki, Practical experience with hole-Free phase plates for Cryo electron microscopy, Microsc. Microanal. 22 (6) (2016) 1316–1328, https://doi.org/10.1017/S143192761601196X.
[26] R. Pretzsch, M. Dries, S. Hettler, M. Spiecker, M. Obermair, D. Gerthsen, Investigation of hole-free phase plate performance in a TEM by experiment and simulation, In preparation.